Unclassified

SECURITY CLASSIFICATION OF THIS PAGE

REPORT DOCUMENTATION PAGE

DTIC FILE COPY

AD-A210 337

DTIC ELECTE JUL 05 1989 D

1b. RESTRICTIVE MARKINGS

3. DISTRIBUTION/AVAILABILITY OF REPORT
Approved for public release; Distribution Unlimited.

HEDULE

4. PERFORMING ORGANIZATION REPORT NUMBER(S)
GL-TR-89-0164

5. MONITORING ORGANIZATION REPORT NUMBER(S)

6a. NAME OF PERFORMING ORGANIZATION
Geophysics Laboratory

6b. OFFICE SYMBOL (*If applicable*)
PHP

7a. NAME OF MONITORING ORGANIZATION

6c. ADDRESS (*City, State, and ZIP Code*)
Hanscom AFB
Massachusetts 01731-5000

7b. ADDRESS (*City, State, and ZIP Code*)

8a. NAME OF FUNDING/SPONSORING ORGANIZATION

8b. OFFICE SYMBOL (*If applicable*)

9. PROCUREMENT INSTRUMENT IDENTIFICATION NUMBER

8c. ADDRESS (*City, State, and ZIP Code*)

10. SOURCE OF FUNDING NUMBERS

PROGRAM ELEMENT NO.	PROJECT NO.	TASK NO.	WORK UNIT ACCESSION NO
62101F	7601	22	01

11. TITLE (*Include Security Classification*)
The Space Radiation Environment at 840 KM

12. PERSONAL AUTHOR(S)
E.G. Mullen, M.S. Gussenhoven, D.A. Hardy

13a. TYPE OF REPORT	13b. TIME COVERED	14. DATE OF REPORT (*Year, Month, Day*)	15. PAGE COUNT
Reprint	FROM _____ TO _____	1989 June 27	14

16. SUPPLEMENTARY NOTATION
Reprinted from AIP Conference Proceedings 186 - High-Energy Radiation Background in Space
Sanibel Island, FL 1987

17. COSATI CODES		
FIELD	GROUP	SUB-GROUP

18. SUBJECT TERMS (*Continue on reverse if necessary and identify by block number*)
Radiation Belts, Dose, Solar Proton Events, Single Event Upsets, Outer Zone Electrons

19. ABSTRACT (*Continue on reverse if necessary and identify by block number*)

The Defense Meteorological Satellite Program (DMSP) F7 satellite, launched in November, 1983, carries a dosimeter provided by the Air Force Geophysics Laboratory. The dosimeter uses planar silicon detectors behind four thicknesses of aluminum shielding to measure both radiation dose and high energy particle fluxes in the space radiation environment at 840 km. Energy thresholds in the detectors are set to distinguish low (electron), high (proton), and very high (>40 MeV) energy particle depositions. The dosimeter returns accurate, high-time-resolution dose measurements. Maps of the radiation dose (electron and proton) at 840 km are presented and compared to the NASA models. Maps of the very high energy deposits which can produce Single Event Upsets (SEUs) in microelectronic components are also presented. Characteristics of energetic particles that enter the polar cap regions during solar particle events are discussed and compared to inner belt proton and cosmic ray background levels. Included is an analysis of two of the largest solar proton events since launch of the satellite, those of 16 February, 1984, and 26 April, 1984.

89 7 03 109

20. DISTRIBUTION/AVAILABILITY OF ABSTRACT
☐ UNCLASSIFIED/UNLIMITED ☒ SAME AS RPT. ☐ DTIC USERS

21. ABSTRACT SECURITY CLASSIFICATION
Unclassified

22a. NAME OF RESPONSIBLE INDIVIDUAL	22b. TELEPHONE (*Include Area Code*)	22c. OFFICE SYMBOL
M.S. Gussenhoven	(617) 377-3212	PHP

DD FORM 1473, 84 MAR

83 APR edition may be used until exhausted.
All other editions are obsolete.

SECURITY CLASSIFICATION OF THIS PAGE

Unclassified

GL-TR-89-0164

AIP
CONFERENCE
PROCEEDINGS 186

RITA G. LERNER
SERIES EDITOR

HIGH-ENERGY RADIATION BACKGROUND IN SPACE

SANIBEL ISLAND, FL 1987

EDITORS:

A. C. RESTER, JR.
UNIVERSITY OF FLORIDA

J. I. TROMBKA
GODDARD SPACE
FLIGHT CENTER

AMERICAN INSTITUTE OF PHYSICS NEW YORK 1989

THE SPACE RADIATION ENVIRONMENT AT 840 KM

E.G. Mullen, M.S. Gussenhoven and D.A. Hardy
Air Force Geophysics Laboratory, Hanscom AFB, MA 01731

ABSTRACT

The Defense Meteorological Satellite Program (DMSP) F7 satellite, launched in November, 1983, carries a dosimeter provided by the Air Force Geophysics Laboratory. The dosimeter uses planar silicon detectors behind four thicknesses of aluminum shielding to measure both radiation dose and high energy particle fluxes in the space radiation environment at 840 km. Energy thresholds in the detectors are set to distinguish low (electron), high (proton), and very high (>40 MeV) energy particle depositions. The dosimeter returns accurate, high-time-resolution dose measurements. Maps of the radiation dose (electron and proton) at 840 km are presented and compared to the NASA models. Maps of the very high energy deposits which can produce Single Event Upsets (SEUs) in microelectronic components are also presented. Characteristics of energetic particles that enter the polar cap regions during solar particle events are discussed and compared to inner belt proton and cosmic ray background levels. Included is an analysis of two of the largest solar proton events since launch of the satellite, those of 16 February, 1984, and 26 April, 1984.

I. INTRODUCTION

A sensitive volume in living tissue can be affected by energy deposition from high-energy particles to such a degree that a person's performance can be degraded or impaired. As such satellite-borne humans are subject to radiation effects as they are carried through naturally occurring or artificially-produced regions of radiation in space. The effects can be produced in three general ways, by total dose, dose rate, and single event upsets (SEUs). As the frequency and duration of manned space flights increase, we need to improve our ability to predict and model the space radiation environment to ensure the safety and maintain the performance capabilities of the crew members.

There are essentially three near-Earth radiation regions: a) the inner radiation belt region populated mainly by stably-trapped high energy protons; b) the outer radiation belt region populated mainly by trapped, but highly variable fluxes of electrons; and c) the polar regions populated mainly by steady galactic cosmic rays and infrequent but high intensity solar proton event particles. Low altitude vehicles in high inclination orbits encounter parts of all the various radiation environments, the extent depending on the altitude of the satellite.

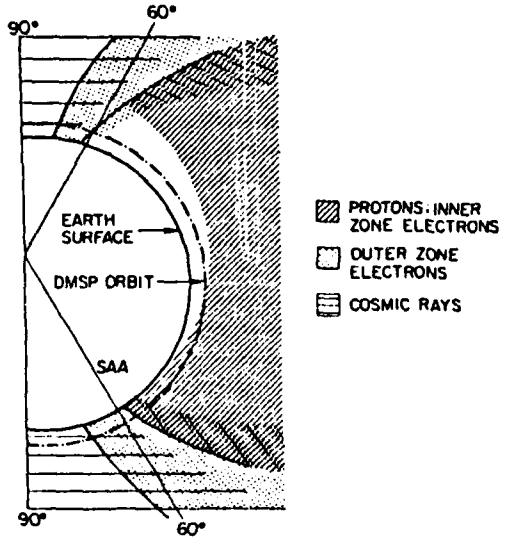

Fig. 1. Schematic diagram of the DMSP polar orbit passing through the low altitude extensions of the major radiation regions. The shading code for the various regions is given on the right.

DMSP/F7 is a three-axis stabilized satellite in a sun-synchronous orbit whose orbital plane is the 1030-2230 local time meridian. The spacecraft altitude is 840 km, its period is 101 minutes, and its inclination is 98.7°. Figure 1 schematically illustrates the three high energy particle populations as they are encountered by the DMSP satellite. The offset of the Earth's

© 1989 American Institute of Physics

dipole is exaggerated to illustrate the low-altitude extension of the proton belts. The stable inner zone proton belt (cross-hatching) reaches low altitudes in the region of the South Atlantic Anomaly (SAA) due to the Earth's offset dipole. The SAA is limited in longitude and latitude, and as the Earth rotates underneath the satellite, approximately 10 of 14 of the daily orbits encounter portions of the SAA. The outer zone electrons (dotted region) are located in two high latitude rings at 840 km, one in each hemisphere. The outer zone fluxes are highly variable. The polar caps (horizontal lines) are regions of direct entry for high energy particles both galactic cosmic rays and solar particles; however, under certain conditions, the higher energy cosmic rays and solar particles can penetrate to 840 km at any latitude.

Of the three regions of high energy particles, two are considered most hazardous to man. They are the SAA and the polar regions during solar particle events. Significant dose in these regions is produced by high-energy protons and heavy ions, which are difficult, or impossible, to shield. The outer zone electrons are lower in energy and can be effectively shielded; however, they are highly variable in intensity and can produce hazardous dose rates behind minimal shielding, such as would be the case for an astronaut only protected by a space suit. The human effects of the higher energy heavy ion particles are not yet fully understood, although it is known that they can produce light flashes in the eyes and may be able to upset certain brain functions, similar to a SEU in a microelectronic chip.

The DMSP dosimeter is extremely versatile, returning information on electron and proton dose, electron and proton flux, and nuclear star events, all with 4 second time resolution and in 4 integral energy steps. It is our intention here to show the versatility of the instrument, and to present results from the major analysis efforts undertaken to date using the dosimeter data. These efforts include both short-term and empirical model results of dose and nuclear star events, as well as case studies of major solar particle events. The dose model results are compared to the NASA model predictions. The short-term results are presented to indicate the range over which the environment can deviate from the models (both ours and NASAs), and where the deviations are likely to be most important. Because of the capability of the dosimeter, we are able to present our direct dose and dose rate measurements separately for electrons and protons.

II. SSJ[4] INSTRUMENT DESCRIPTION

The DMSP/F7 dosimeter measures the radiation dose from both electrons and protons occurring behind four different thicknesses of aluminum shielding. Additionally, information is provided on the differential and integral fluxes of electrons and protons at energies above the thresholds defined by the shields, and on the number of nuclear star events in each detector. The basic measurement technique is the determination of the amount of energy deposited in a simple solid-state detector from particles with sufficient energy to penetrate the shielding. A lower limit cutoff of 50 keV is set for measuring energy deposition in each detector. Each of the four detectors is mounted behind a hemispheric aluminum shield. The aluminum shields are chosen to provide electron energy thresholds for the four sensors of 1, 2.5, 5, and 10 MeV, and for protons of 20, 35, 51, and 75 MeV. The 1 MeV threshold sensor has a detector area of .051 cm^2, and the remaining three each have areas of 1.00 cm^2. Particles that penetrate the shield and bremsstrahlung produced in the shield will deposit energy in the device producing a charge pulse. The charge pulse is shaped and amplified. The pulse height is proportional to the energy deposition in the detector, and the dose is proportional to the sum of the pulse heights.

Energy depositions in the range between 50 keV and 1 MeV are used to calculate the low linear energy transfer (LOLET) dose; depositions between 1 MeV and 10 MeV provide the high linear energy transfer (HILET) dose; energy depositions above 75 MeV in detector 3 and above 40 MeV in detectors 1, 2, and 4 are counted as very high linear energy transfer (VHLET) events. The LOLET dose (which we will call electron dose below) results primarily from electrons, high energy protons (above approximately 100 MeV incident), and bremsstrahlung. The HILET dose (which we will call proton dose below) comes primarily from protons below about 100 MeV incident and above the dose threshold for each detector. The integral flux is proportional to the number of energy depositions counted. The VHLET counts (which we will call "star counts" below) come from a.) high energy nuclear (mostly proton induced) interactions inside and /or near the sensitive device volume, b.) direct energy deposition by heavier cosmic rays, or c.) direct energy deposition by protons that have long path lengths in the detectors. These will be referred to respectively as a.) nuclear stars, b.) cosmic ray events and c.) direct deposit proton events below. (The 'star'

TABLE 1

DMSP/F7 J[4] DOSIMETER CHARACTERISTICS

Dome	Aluminum Shield	Dome Thresholds Electron	Proton	Area	Detector Thickness	Threshold LOLET	HILET	VHLET
	($\mu g/cm^2$)	(MeV)	(MeV)	(cm^2)	(microns)	(MeV)	(MeV)	(MeV)
1	0.55	1	~20	.051	398	.05-1	1-10	>40
2	1.55	2.5	35	1.000	403	.05-1	1-10	>40
3	3.05	5.0	51	1.000	390	.05-1	1-10	>75
4	5.91	10.0	75	1.000	384	.05-1	1-10	>40

Dist | Special
A-1 | 20

description originally comes from the array of emulsion tracks observed when a high energy proton interacts with a nucleus producing secondaries and a recoiling fragment.) Thus, five separate outputs are obtained from each of the four hemispherically shielded detectors: LOLET (electron) dose, LOLET (electron) flux, HILET (proton) dose, HILET (proton) flux, and VHLET flux (star counts). (A complete description of the instrument can be found in Gussenhoven et al.[1]) A summary of the detector properties and their shielding is given in Table 1, and a summary of the dome shielding effectiveness for protons is given in Table 2.

TABLE 2

DOME SHIELDING EFFECTIVENESS FOR PROTONS

INTERNAL PROTON ENERGY (MeV)	EXTERNAL PROTON ENERGY (MeV)			
	DOME 1	DOME 2	DOME 3	DOME 4
0	20.0	35.0	51.0	75.0
8	21.8	37.0	52.5	75.2
10	23.4	37.8	53.0	75.7
20	30.0	43.0	56.8	78.5
40	45.0	55.0	68.0	87.5
100	103.2	110.0	119.0	124.2
1000	1001.	1003.	1005.	1010.

III. DOSE MEASUREMENTS AND MAPS

During quiet times when there are no high energy solar protons present, the high energy proton fluxes are measured by DMSP/F7 dosimeter only in the SAA. A survey of the satellite's daily encounters of the SAA is shown in Figure 2. Here the average flux count rates for protons >75 MeV are plotted as a function of universal time (UT) in hours for 9 November 1984. The averaging interval is one minute. Each spike in the count rate indicates the crossing of a portion of the SAA as the Earth rotates underneath the DMSP orbit. Between each crossing, the satellite passes over the two polar caps and the equatorial region opposite the SAA. During these intervals, only background counts are detected. Similar spatial distributions occur for the lower energy proton flux counts and the proton dose counts.

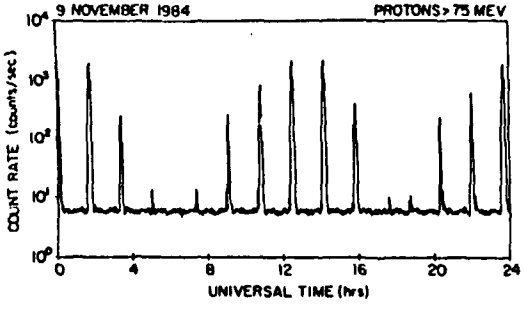

Fig. 2. Proton flux counts for energies greater than 75 MeV, measured by DMSP on 9 November 1984 when no solar event was in progress. The spikes occur during crossings of the South Atlantic Anomaly.

The depth-dose spectra for the electron, proton and total dose, obtained from a single traversal through the heart of the SAA on February 3, 1985, are given in Figure 3. The spectra are hard (highly energetic), with the dose decreasing only somewhat more than a factor of two over the entire shielding range and becoming nearly asymptotic for the thickest shielding. The proton dose is approximately twice the electron dose. The total dose behind the thinnest shield is .38 rad(Si) and behind the thickest shield is .17 rad(Si). For the DMSP satellite, the total dose per day from the SAA is nearly 2 rad(Si) behind the thinnest shield and 1 rad(Si) behind the thickest shield.

To make a more quantitative estimate of the dose accumulated per day from the SAA we constructed an empirical DMSP dose rate map for 840 km altitude. Dose count-rates from individual passes were accumulated for a full year (from 1 November, 1984 to 31 October, 1985) in bins five degrees by five degrees wide in corrected geomagnetic latitude and longitude coordinates. Average count rates were calculated for each bin, and contours of constant dose drawn. The dose rate map for the >75 MeV HILET channel (with 5.91 g/cm^2 aluminum shielding) is shown in Figure 4. The map is in corrected geomagnetic coordinates. The contours are in rad(Si) per day. As can be seen, the only significant proton dose occurs in the SAA where the contours range from 0.1 to 10 rad(Si) per day.

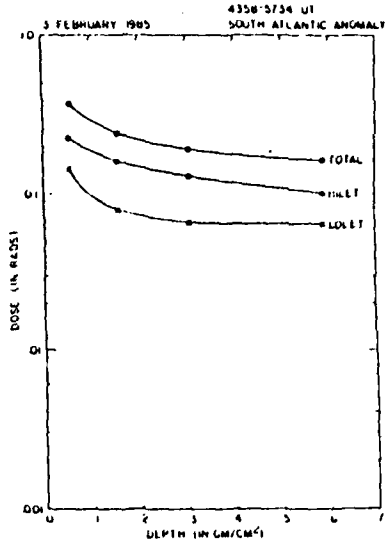

Fig. 3. Depth-dose spectrum for a DMSP/F7 crossing of the heart of the South Atlantic Anomaly on 3 February, 1985.

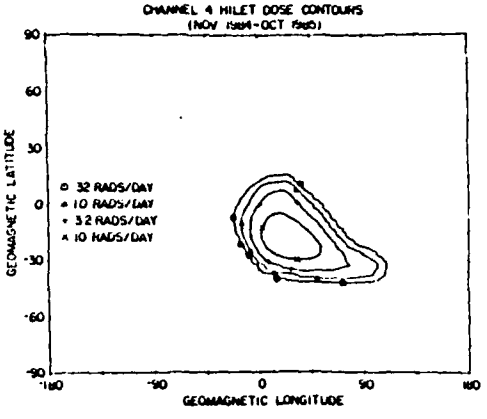

Fig. 4. Contours of constant dose-rate for the > 75 MeV proton dose detector, plotted in corrected geomagnetic latitude and longitude coordinates.

The outer zone electrons are mostly found at magnetic latitudes between 50° and 70° at 840 km. The extent of these zones is shown in Figure 5, which is the DMSP dose rate map for electron detector 1 (behind 0.55 g/cm^2 shielding). The outer zone electron dose is very evident and appears as two high latitude bands. The SAA is also apparent; however, in the SAA the dose results from a combination of electrons above threshold energies (>1 MeV) and protons with energy greater than ~100 MeV.

To show how the DMSP measured dose compares with the NASA model values, Table 3 gives a listing of individual day and yearly average proton and electron dose/day obtained from DMSP and the NASA model predictions for the same orbit for both solar maximum and solar minimum options. The first three measured values result from summing the DMSP dose counts for the three individual days: 9 November 1984, 26 November 1984, and 3 February 1985, respectively. There were no solar proton events on these days. The average DMSP values result from running nine successive days of DMSP/F7 orbits through the DMSP dose rate map values and taking the average accumulation. The standard deviation varied from ±8% in the first proton detector up to ±10% in the highest energy detector. The standard deviations are listed just below the average DMSP values. Similarly the DMSP/F7 satellite orbit was run through appropriate NASA radiation belt models for solar maximum and solar minimum conditions with the dose calculated at the center of a solid aluminum sphere of

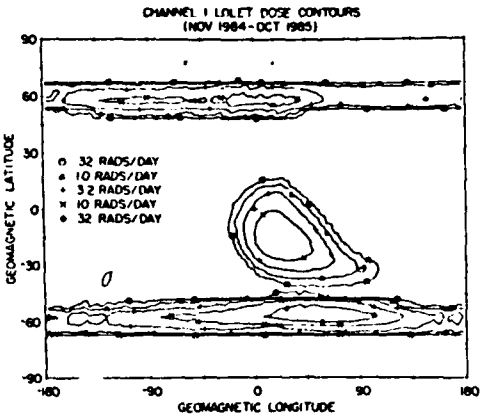

Fig. 5. Contours of constant dose-rate for the >1 MeV electron dose detector, plotted in corrected geomagnetic latitude and longitude coordinates.

thickness equal to the DMSP dosimeter shielding values. The NASA model values for solar minimum and maximum are given at the bottom of the table. (Details of the NASA models can be found in Singley and Vette[2], Teague and Vette[3], and Sawyer and Vette[4], and problems associated with radiation belt modelling can be found in Vette et al.[5])

TABLE 3

COMPARISON OF NASA MODEL AND DMSP DOSE VALUES

	PROTONS RAD(SI)/DAY				ELECTRONS RAD(SI)/DAY			
DETECTOR NO	1	2	3	4	1	2	3	4
DAY 11/09/84	1.20	0.83	0.63	0.48	1.61	0.35	0.28	0.27
DAY 11/26/84	1.22	0.77	0.57	0.44	13.02	0.50	0.27	0.28
DAY 2/03/85	1.18	0.80	0.59	0.46	6.31	0.35	0.26	0.26
AVERAGE	1.21	0.83	0.63	0.49	2.51	0.34	0.26	0.27
STANDARD DEVIATION	±8%	±9%	±9%	±10%	±2%	±9%	±9%	±9%
NASA SOLAR MIN	1.28	0.70	0.49	0.20	10.83	0.58	0.03	0.00
NASA SOLAR MAX	0.89	0.47	0.33	0.18	11.62	1.28	0.07	0.00

SOLAR MIN = AP8MIN, AE5MIN, AE17LO
SOLAR MAX = AP8MAX, AE6MAX, AE17HI
NASA MODEL PROPAGATED THROUGH A SOLID ALUMINUM SPHERE

For the proton dose, the DMSP individual day and DMSP average values are approximately the same. They all agree to within 10%, which is the same variation found in the day to day orbital runs. This indicates that the proton radiation belts are very stable over the one-year duration of the data acquisition, as expected. The solar minimum NASA model values when compared to the near-solar minimum DMSP values for proton dose are only slightly higher for the thinnest shielding and are only slightly lower for the remaining thicknesses. The agreement is felt to be remarkably good given the differences in measurement techniques and solar cycles, and indicates the long term stability of the inner belt.

For the electron dose, the directly measured daily dose varies greatly, from 1.6 to more than 13 rad(Si) behind the thinnest shielding. For higher shielding the dose is relatively constant. The average DMSP model value is 2.51 rad(Si) for the thinnest shielding. This indicates the high variability of the outer zone electrons, over time periods much less than one year. Furthermore, the comparison of the DMSP model and NASA model values is poor. The dose calculated for the DMSP orbit from the NASA models is higher by factors of 4 and 1.8 for Channels 1 and 2, respectively. For the last two channels, the DMSP directly-measured and model electron dose values are nearly constant, while the NASA model values fall to zero. This behavior results from bremsstrahlung effects in the DMSP measured values which would not be predicted from electron fluence in the NASA model values. While it is possible that on occasion (i.e., 26 November, 1984) the daily measured electron dose in Detector 1 can be higher than that predicted by the NASA models, the Detector 2 measured values have not been observed to be as large as the NASA model values. We conclude that the NASA models for electrons are both too high in intensity and too hard in spectral shape.

Comparing total dose behind the thinnest shielding for the DMSP/F7 orbit on a yearly basis,

the NASA models give values that are too high by somewhat more than a factor of 3 for the 1984 period. The electron contribution to the total dose is the major source of the discrepancy. Below we will more closely examine the highly variable electron dose from the DMSP data set.

In order to quantify the high variability in outer zone electron fluxes we constructed a daily averaged flux count rate using the region in space where the maximum fluxes occur. Figure 5 illustrates that the maximum occurs in the southern hemisphere in a rectangle centered near -55° geomagnetic latitude and 55° geomagnetic longitude. The region lies far enough below the SAA to avoid contamination of the flux and dose measurements from protons. All flux count rates which fall in this rectangular region were averaged for one day intervals to show the variability of the outer zones. In Figure 6 the average flux count rate for electrons with energy >2.5 MeV is plotted as a function of day number for 1984, the first full year of the dosimeter operation. The day numbers are marked off in 27-day solar rotation units. The average count-rates vary over more than two orders of magnitude, and high fluxes can persist for many days on end. The 27-day recurrence of outer zone electron enhancements is particularly evident in the three largest events in the last quarter of the year.

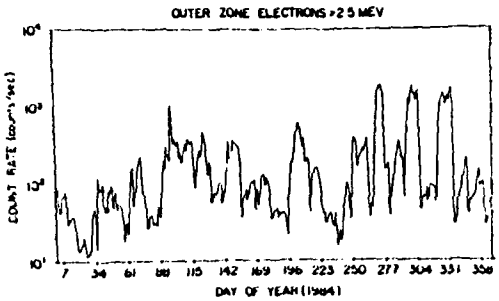

Fig. 6. Daily average count-rates for the >2.5 MeV outer zone electrons plotted as a function of day number for 1984.

IV. STAR COUNT MEASUREMENTS AND MAPS

To perform meaningful statistical analyses of the star count (VHLET) particles, the data must be separated into appropriate regions of space. For this study, the data are summed over all longitudes in broad latitudinal ranges designated as the North Pole (NP) from 40° N to 90° N, Middle Latitude (ML) from 15° N to 40° N, South Atlantic Anomaly (SAA) from 55° S to 15° N and South Pole (SP) from 55° S to 90° S.

Figure 7 shows the average daily star count rates for dosimeter detectors 1 and 2 for 1984 plotted versus day of the year in each of the 4 latitudinal bins. Similarly Figure 8 shows the count rates for detectors 3 and 4. The sharp peaks in the polar cap regions are due to solar particle events. Only 3 solar particle events of any magnitude occurred in 1984. The flare events seen in the polar regions do not penetrate into the mid-latitude or SAA regions. Aside from these peaks, the data are extremely stable over the year and continue to be stable through 1985 and 1986 where we also have plotted the data (not shown). The 1984 through 1986 data were all collected during solar minimum conditions.

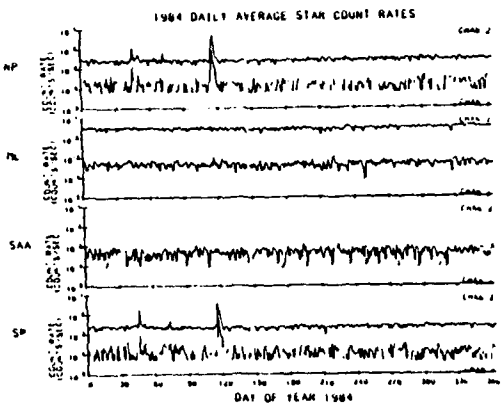

Fig. 7. 1984 daily average star channel counts for detectors 1 and 2.

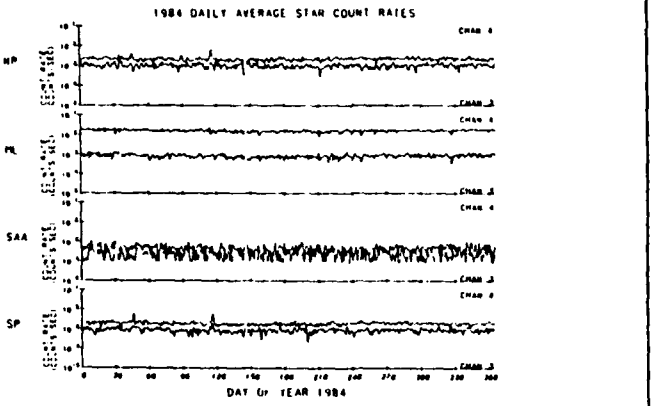

Fig. 8. 1984 daily average star channel counts for detectors 3 and 4.

Figures 9 and 10 show the occurrence frequency of star counts in map format for detectors 2 and 3 of the dosimeter respectively. (Maps for detectors 2 and 4 and additional information on the star counts are provided in Mullen et al.[6]) Shown in gray scale are the average star count rates (counts/s) for the period from November 1984 through October 1985. The average has been calculated for each one degree geographic latitude and longitude box. The gray scale extends from 10^{-3} counts per second to greater than .05 counts per second in logarithmic intervals. The gray scale code is displayed to the right of the pictures. Small holes (data gaps) in the maps occur because the satellite orbit is synchronized with the Earth's rotation resulting in incomplete coverage of all 1^{o} by 1^{o} bins. The maps provide information on the particle populations producing the high energy deposits which will be discussed below.

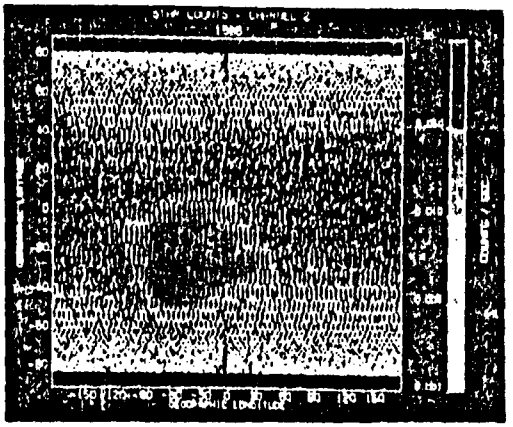

Fig. 9. Gray scale plot of star count rates for detector 2.

The general features pictured in both Figures 9 and 10 may be summarized as follows: a.) highest count rates occur in the region of the South Atlantic Anomaly where the inner radiation belt particles extend down to DMSP altitudes; b.) next highest count rates occur in the polar regions where solar protons and heavy ions have direct access along magnetic field lines down to lower altitudes; and c.) scattered count rates occur at all locations. This means that the highest LET particles might be expected any place in an 840 km orbit but the highest probability is in the region of the SAA, where it is proton dominated.

Information on the characteristics of the particles producing the counts can be obtained by statistically examining individual counts and count rates and the ratios of counts in the different detectors. To avoid mixing regions having different characteristics, all the statistics were done in the 4 latitude bins discussed above. Table 4 gives the total VHLET counts and average yearly count rates. Approximately 312 equivalent full days of data between November 1984 and October 1985 were used to calculate the yearly averages. During this period, no solar proton events were seen in the data. Table 5 gives the yearly average count rate ratios for these 4 regions for each detector.

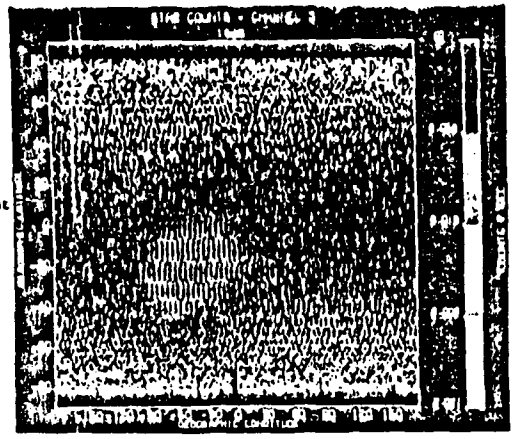

Fig. 10. Gray scale plot of star count rates for detector 3.

TABLE 4

TOTAL STAR COUNTS AND COUNT RATES

	TOTAL COUNTS			
LATITUDE BIN	DET 1	DET 2	DET 3	DET 4
NP	1164	19813	8408	17884
ML	121	2100	893	2015
SAA	5889	335641	10714	201530
SP	897	15329	6615	13979

	COUNT RATES (COUNTS/SEC)			
LATITUDE BIN	DET 1	DET 2	DET 3	DET 4
NP	1.5E-04	2.6E-03	1.1E-03	2.3E-03
ML	3.1E-05	5.3E-04	2.3E-04	5.1E-04
SAA	5.3E-04	3.0E-02	9.6E-04	1.8E-02
SP	1.7E-04	2.8E-03	1.2E-03	2.6E-03

TABLE 5

DETECTOR STAR COUNT RATE RATIOS IN LATITUDE BINS

	DETECTOR RATIOS		
LATITUDE BIN	3/1	2/1	2/4
NP	7.22	17.0	1.11
ML	7.38	17.4	1.04
SAA	1.82	57.0	1.67
SP	7.37	17.1	1.10

As mentioned above, star counts can be produced directly by proton energy deposition, directly by cosmic rays, and/or indirectly by nuclear star events in or near the detectors. In order for the protons to directly produce a pulse in the detector, they must have sufficient path length in the detector and sufficient energy to deposit energy above the threshold level (≈40 MeV or ≈75 MeV depending on the detector). Because the detectors are planar, they have small lateral dimensions such that there is only a very narrow angular and energy range of particles that can produce pulses by direct deposition. In detectors 1 and 3 no pulses can be produced by direct proton energy deposit since the total path length is too short for any energy proton to produce a pulse of the required size to be counted. In detectors 2 and 4, only protons incident between approximately 87.5° and 90° with external energies between approximately 55 MeV and 58 MeV for detector 2 and between approximately 85 MeV and 88 MeV for detector 4 can produce pulses of the required magnitude to be counted. Protons below these energies do not have sufficient energy to produce VHLET size pulses, and protons above these energies will pass through the detectors without depositing sufficient energy. Particles at 0° incidence must have a mass of oxygen or

greater to produce a VHLET pulse. Particles with masses less than oxygen (such as helium) must be incident at an angle less than the normal to produce a pulse. The differences in the shielding, detector area, and response characteristics of the 4 detectors will be used to gain insight into the properties of the particles creating the pulses.

Since detectors 1 and 3 do not measure any counts due to direct energy deposition by protons, the counts in these two detectors are produced only by nuclear star events and direct cosmic ray events with appropriate masses and incident angles. Star counts in the Middle Latitude (ML) region are almost entirely due to extremely high energy cosmic rays since the geomagnetic cutoff of the Earth's magnetic field prohibits normal solar protons from directly entering into this region of space. We also know that the star counts in the South Atlantic Anomaly (SAA) region are due almost entirely to protons from the inner belt trapped particle population. In Table 5 the ratios of star counts of channels 3 to 1, 2 to 1 and 2 to 4 are listed. By comparing ratios from the polar regions (NP and SP) to the ML and SAA ratios, it is evident that the polar region ratios are the same as (within statistical error) those of the middle latitude region. We conclude that since the ratios are the same, the counts are produced by the same type of particles, namely cosmic rays. This is not unexpected since high energy cosmic rays have their most direct access into the near-Earth environment down the open magnetic field lines in the polar regions.

If we assume that the numbers of high energy deposits produced by particles of the same energy is directly proportional to the area of the detectors, we can use the ratio of star counts from detectors 1 (40 MeV threshold) to those from detector 3 (75 MeV threshold) to get a first order feel for the relative upset susceptibility in space for materials (tissues) that might have different sensitivity thresholds. The ratio of the area of detector 1 to detector 3 is 19.6. The 3/1 channel ratio for the poles is ~7.3 and for the SAA is 1.82. This indicates that the relative upset susceptibility of materials with a 40 MeV threshold to materials with a 75 MeV threshold is approximately 3 times as great in a cosmic ray environment and 11 times as great in the South Atlantic Anomaly if the materials are proton sensitive.

We can separate nuclear stars from direct deposits in detector 2 by comparing the data from detectors 1 and 2. We know that detector 1 responds only to nuclear stars and detector 2 responds to both nuclear stars and direct proton deposition in the region of the SAA. The number of nuclear stars (statistically speaking) in detector 2 should differ from those in detector 1 primarily by the relative detector area factor of ~19.6. The shielding difference between the two detectors however, reduces this factor somewhat. From Table 5 it can be seen that factor is ~17.4 for the cosmic ray dominated middle latitude region. For the proton dominated SAA region, the factor could be more or less than the 17.4 depending on the shape of the proton spectrum, but could not be significantly different. Subtracting the estimate of the detector 2 nuclear stars (determined by multiplying detector 1 by 17.4) from the total detector 2 counts in Table 4 shows that for the SAA region the direct deposit protons in detector 2 are, on the average, approximately a factor of 2 greater than the nuclear star counts.

Since detectors 2 and 4 differ only in their shielding thickness, their areas and detector thresholds being the same, shielding effectiveness can be estimated by examining the counts ratio of these two detectors. In the mid-latitude and polar regions where the higher energy cosmic rays dominate, the shielding effectiveness is only 10% or less. In the SAA where the protons dominate, the shielding effectiveness is much greater because the energetic proton spectrum is softer. Even in the SAA region, there are major differences in the hardness of the spectra as a function of position. Figure 11 shows the ratio of average star count rates for detector 2 to detector 4 for the period from November 1984 through October 1985 in one degree geographic latitude and longitude boxes. The ratios are gray scale coded to indicate ranges from 1 to ∞ in logarithmic type intervals. The gray scale code is displayed to the right of the figure. The

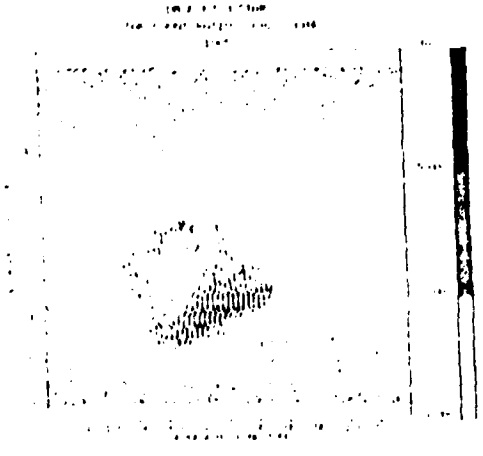

Fig. 11. Gray scale plot of star count ratios of detector 2 to detector 4.

gradual shift in the ratio across the South Atlantic Anomaly region is due to the magnetic field strength (L-Shell) variation. Higher energy particles are able to diffuse further inward across magnetic field lines, thus reaching lower L values and producing a harder spectrum at the lower L values.

V. THE SOLAR PARTICLE EVENTS OF 16 FEBRUARY AND 25-29 APRIL, 1984

The two largest solar particle events during 1984 occurred in February and April. Figures 12a and 12b are survey plots of the DMSP flux count data for protons >75 MeV (the highest energy channel) . the peak days of the two events: 16 February and 26 April, respectively. They are in the same format as Figure 2. In each plot, three types of counts can be identified: background counts; the systematically occurring SAA flux counts that stood alone in Figure 2; and the large flux levels across each of the polar regions. The latter are solar protons and heavy ions which have direct access to low latitudes in the polar regions. On 16 February there is a sudden onset of solar particles in the caps at ~09 UT. The fluxes fall by an order of magnitude within 4 hours, after which there is a steady exponential decay of the particles that continues into the 17th. At the beginning of 26 April the high energy precipitation into the polar caps was already in progress. This event had a much slower buildup and decay. The widths of the flux peaks in the polar regions show that during solar proton events significant dose can be received at polar orbiting vehicles. Even in these survey plots one can discern significant spatial and/or temporal variations in the cap fluxes. They are particularly large at the beginning of the 16 February event.

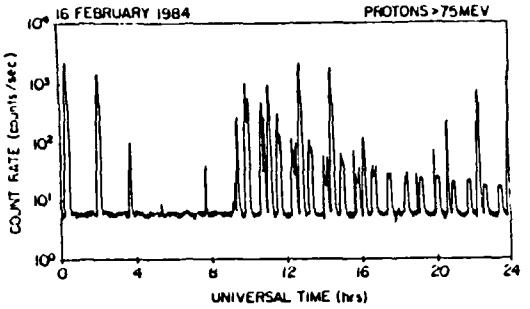

Fig. 12a. Daily plot of one-minute-averaged flux count rate for protons with energy greater than 75 MeV on 16 February, 1984.

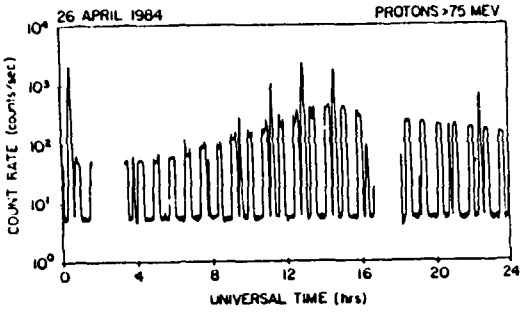

Fig. 12b. Daily plot of one minute averaged flux count rate for protons with energy greater than 75 MeV on 26 April, 1984.

To show the kind of variability that exists across the polar cap during solar events, the paths of two polar crossings on 16 February are shown in Figure 13. Here the satellite track is plotted in corrected geomagnetic latitude (MLAT)-magnetic local time (MLT) coordinates. The length of the black lines vertical to the track represents the count rate in the lowest energy proton channel (>20 MeV). These plots show a) the low latitude cutoffs (<60° MLAT) of the solar particles; b) that the particles fill both the regions normally occupied by the outer zone electrons and the polar cap; c) that relatively deep troughs occur in the flux levels which are located differently in the northern and southern hemispheres, but are near the magnetospheric cusp. Because the variations in electron and proton fluxes (not shown) are so similar in the 16 February event, it is very likely the case that the "electron" count rates contain a significant contribution from the >100 MeV protons.

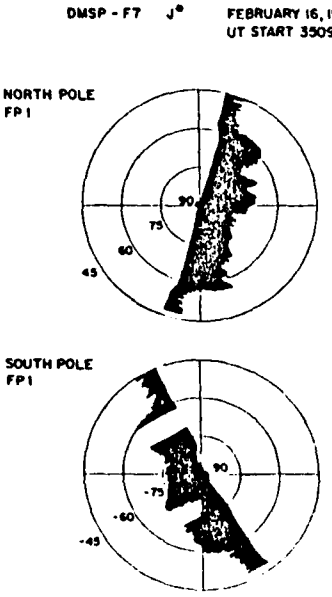

Fig. 13. Polar plots of the >20 MeV protons during the peak of the 16 February event. The coordinates are corrected geomagnetic latitude and geomagnetic local time.

Since the shape of the spectra are very important in assessing damage during solar events, the proton flux counts are used to find an average power law spectrum for protons for each flare. For the 16 February data, at the peak of the proton flux the optimal spectral fit for the counts averaged across the polar cap is:

16 February (peak): $j(E) = 86(\pm 2) \times (20/E)^{1.8}$ p/cm^2-s-MeV,

where E is in MeV. Under the assumption of complete particle isotropy in the upward hemisphere at DMSP altitudes and integrating from 10 MeV to infinity, the directional integral flux from the equation above is 298 p/cm^2-s-sr. The average spectrum for 17 February, using the cap data for the entire day is:

17 February: $j(E) = 0.85\ (\pm 0.05) \times (20/E)^{2.7}$ p/cm^2-s-MeV.

Because the solar event in April is so slowly varying we list the spectra determined by averaging the cap data for each day from 25 - 28 April. They are:

24 April:	Background levels
25 April:	$j(E) = 5.6\ (\pm 0.4) \times (20/E)^{3.0}$ p/cm^2-s-MeV
26 April:	$j(E) = 116\ (\pm 4.0) \times (20/E)^{3.8}$ p/cm^2-s-MeV
27 April:	$j(E) = 6.8\ (\pm 0.4) \times (20/E)^{4.3}$ p/cm^2-s-MeV
28 April:	$j(E) = 18.\ (\pm 2.0) \times (20/E)^{4.0}$ p/cm^2-s-MeV

The de -tion listed in parenthesis is the uncertainty in the fitting procedure and does not include the instrument's inherent uncertainties. From the power law fits to the flux counts we draw the following conclusions: a) Throughout the February event the spectra were much harder than any of those occurring in the April event. b) The February event softened in time. c) The April event softened over the first three days, then increased in intensity and became slightly harder.

Figures 14a and 14b are the depth-dose spectra for single polar cap crossings during the peaks of the two events. The time intervals were approximately the same for the crossings (21.3 min on 16 February, and 19.2 min on 26 April). In each plot, the electron dose, the proton dose, and their sum are plotted separately for each of the four domes as a function of aluminum shielding thickness (in mass per unit area).

We compare these to the depth-dose spectrum for the SAA crossing (Figure 3) which took 23 min. The depth-dose spectrum for the peak flux on 16 February, Figure 14a, shows that the total dose behind the minimum shielding is 0.2 rad(Si), or somewhat less than in the SAA. The dose source is mainly protons, the electron contribution being less than 25% of the total. The

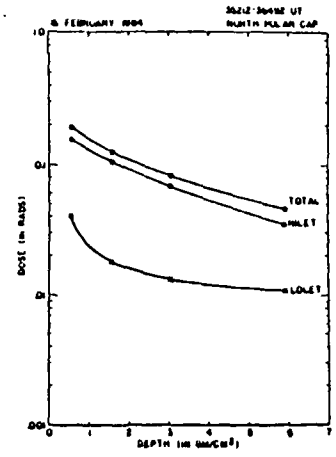

Fig. 14a. Depth-dose spectrum for a DMSP/F7 crossing of the north polar cap at the peak of the solar particle event on 16 February, 1984.

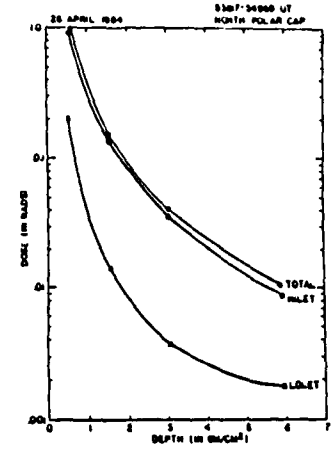

Fig. 14b. Depth-dose spectrum for a DMSP/F7 crossing of the north polar cap at the peak of the solar particle event on 26 April, 1984.

spectrum is falling slowly with increased shielding, but faster than in the SAA indicating a softer (less energetic) particle population. Shielding is still effective at 5.91 gm/cm^2, where the total dose is reduced to 0.05 rad(Si). Since this event decays quickly, the maximum dose behind the minimum shielding is less than 2 rad(Si) over a period of less than one day.

The depth-dose spectrum across the northern polar cap for the peak of the solar particle event on 26 April is shown in Figure 14b. More than 83% of the total dose comes from protons. The spectrum is considerably softer than that in the SAA or at the peak of the 16 February event. It is, however, much more intense at low shielding values. For .55 gm/cm^2 aluminum shielding, 1.2 rad(Si) are received. This falls by two orders of magnitude to 0.012 rad(Si) at maximum shielding (5.91 gm/cm^2) where the dose is approximately an order of magnitude less than encountered in the SAA or in the 16 February event. Shielding remains effective throughout the spectrum. The dose per polar crossing remained high for several days, and in the first three days the total dose exceeded 25 rad(Si) for .55 gm/cm^2 of aluminum shielding. This is more than four times the dose received in the same time period and behind the same shielding from the SAA.

The dosimeter star data can also be used to study solar proton events. Here we examine the entire periods of the February and April 1984 solar particle events seen in Figures 1 and 2. The peaks of the events were on 16 February 1984 and 26 April 1984. Since the events are only seen in the polar regions, only the polar region data is used. The two polar cap regions were added together to get better statistics for the event days. Table 11 gives the daily average of star

channel count rates for the 4 detectors in counts per second times 10^{-4} for the periods 15-17 February 1984 and 24-30 April 1984. Also given are the 1985 average count rates for comparison as a normal background level and the differences from the 1985 averages for the days of interest. The count rates were determined only from the polar regions: between 40° and 90° North Latitude and 55° and 90° South Latitude. Data equatorward of 55° South Latitude were excluded from the table to prevent contamination from the SAA. It is obvious that during the events the number of energetic particles that can produce 40 MeV pulses (detectors 1, 2, and 4) can go up significantly from factors of approximately 2 to 50 depending on shielding thickness. It is also evident that with a shielding equivalent of 3 gm/cm^2 (detector 3), there is less than a factor of 2 increase in particles that can produce a 75 MeV pulse. Subtracting the 1985 average from the star counts on the flare days gives the flare produced numbers shown in the bottom of Table 11. Comparing these back to the 1985 averages shows that in no cases did the flares produce more pulses in detector 3 than the averages, and only at the peak of the events were there more particles seen in detector 4. This says that neither particle event had a spectral hardness at the highest energies greater than the natural cosmic ray background. The softness of the event spectra probably accounts for the fact that unusually high upsets have not been seen on satellites during flare periods to date.

Table 11 Star Count Rates

Count Rates (counts/sec x 10^{-4})

	1985	Feb 84			Apr 84						
DETECTOR	Ave.	15	16	17	24	25	26	27	28	29	30
1	1.6	0.6	12.0	1.8	1.3	9.6	83.0	26.0	9.6	7.9	2.2
2	27.0	28.0	170.0	38.0	27.0	87.0	500.0	190.0	91.0	38.0	27.0
3	11.0	12.0	14.0	8.8	12.0	9.6	18.0	12.0	8.5	7.1	10.0
4	24.0	22.0	53.0	26.0	20.0	25.0	62.0	29.0	22.0	18.0	19.0
					Flare Produced Differences from 1985 Averages						
1		--	10.4	0.2	--	8.0	81.4	24.4	8.0	6.3	0.6
2		1.0	143.0	11.0	--	60.0	473.0	163.0	64.0	11.0	--
3		1.0	3.0	--	1.0	--	7.0	1.0	--	--	--
4		--	29.0	2.0	--	1.0	38.0	5.0	--	--	--

VI. DISCUSSION AND CONCLUSIONS

The dosimeter on the DMSP/F7 satellite has been shown to be a very versatile instrument which can measure energetic particles of different types over a wide dynamic range. It can measure the dose effects of electrons and protons separately, and gives accurate measurements over short time periods. The dosimeter also can distinguish those very high LET particles that can produce SEU type behavior in sensitive materials.

From the data we see that dose accumulated in the SAA is extremely stable, showing no measurable variation from day to day. The SAA contributes 2 rad(Si)/day behind .55 g/cm^2 aluminum shielding. Approximately 60% of the total is dose from protons with energy less than 100-200 MeV, and the remaining 40% is LOLET dose, from electrons, high energy protons (>100-200 MeV) and bremsstrahlung. The depth-dose spectrum for the SAA is very hard, falling only by 60% for shielding thicknesses between .55 and 5.91 gm/cm^2. For non-solar particle event periods, the SAA provides most of the proton dose at DMSP altitudes. The NASA solar minimum proton model for DMSP altitudes predicts a proton dose which is within statistical error of the dose measured on DMSP.

The dose from the outer zone electrons provides the remainder of the daily dose when there are no solar particles from solar proton events. The dose per day from the outer zone electrons is highly variable and large, from 1 to more than 10 rad(Si)/day for .55 gm/cm^2 aluminum. The average electron dose rate determined from the DMSP dose rate model for the year 1984-85 is 2.5 rad(Si)/day. This is four times less than that predicted by the NASA models for solar minimum from electrons alone. The electron depth-dose spectrum is very soft, falling to a near-constant bremsstrahlung level by 3.05 gm/cm^2 aluminum.

Dose effects from the two largest solar particle events in 1984 were measured. The event that occurred on 16 February, 1984, lasted less than a day, had a reasonably hard spectrum, and led to an accumulated dose of less than 2 rad(Si) behind .55 gm/cm^2 aluminum, which is about the same as the SAA-accumulated dose for one day. The event that occurred on 25-29 April, 1984, had a very soft spectrum compared to the SAA and the 16 February spectra. The accumulated dose, however, for a three-day period was larger than that for the SAA behind .55 gm/cm^2 of shielding (25 rad as compared to 6 rad), these levels could prove harmful for an astronaut performing EVA during this period.

For short flights in polar orbit, our results show that a three-day mission at high inclination and at 840 km altitude during moderately large solar particle events could lead to a dose deposition of 30 rad(Si) or more behind minimal spacecraft skin thicknesses which approximate .5 gm/cm^2 aluminum. This level may be sufficient to damage the ocular nerve unless shielded (M.A.

Shea, private communication, 1984). For manned space flights in the polar regions, care must be taken in planning and carrying out activities where minimally shielded astronauts could be exposed to dangerous radiation levels.

For the highest LET particles, the probability of seeing effects in proton sensitive materials is greatest in the region of the SAA. For materials not proton sensitive, the highest probability is in the polar regions. Counts observed outside the polar cap and SAA regions are almost entirely due to higher energy cosmic rays that penetrate beyond the magnetic cutoff region. Although these particles are statistically small, they can appear anywhere in an 840 km orbit.

In conclusion, accurate, short-term models of dose rate are needed for future space missions that are manned for long periods of time, or that rely on new microelectronic technologies. The NASA models projected to low altitude give orbital dose values which are too high by a factor of four during solar minimum. The DMSP proton and electron models, constructed for solar minimum conditions, show that the discrepancy is due to an overestimate of the electron dose. The conservative NASA model predictions can impose more stringent shielding conditions than are necessary. Models of dose in the polar regions during solar proton events do not exist because of the high temporal and hardness variability of the particle fluxes. Nevertheless, significant dose levels can be accumulated during these events and must be taken into account in orbital planning. This can most likely be done on a "worst case" and probability of occurrence basis. It should be remembered that for satellites in near-Earth orbit, the lifetime total dose is mostly accumulated in short bursts and not at a steady constant rate. This leaves much of a satellite system's time in a relatively benign environment during which many of the dose effects can anneal out of certain sensitive materials.

REFERENCES

1. Gussenhoven, M.S., R.C. Filz, K.A. Lynch, E.G. Mullen and F.A. Hanser, Space Radiation Dosimeter SSJ⁴ for the Block 5D/Flight 7 DMSP Satellites: Calibration and Data Presentation, Air Force Geophysics Laboratory, Hanscom AFB, MA, AFGL-TR-86-0065, March, 1986.

2. Singley, G.W. and J.I. Vette, A Model Environment for Outer Zone Electrons, NASA Goddard Space Flight Center, Greenbelt MD, NSSDS 72-13, December, 1972.

3. Teague, M.J. and J.I. Vette, A Model of the Trapped Electron Population for Solar Minimum, National Space Science Data Center, NASA Goddard, NSSDC-74-03, 1974.

4. Sawyer, D.M. and J.I. Vette, AP-8 Trapped Proton Environment for Solar Maximum and Solar Minimum, National Space Science Data Center, NASA Goddard Space Flight Center, Greenbelt MD, WDC-A-R&S 76-06, December, 1976.

5. Vette, J.I., K.W. Chan, and M.J. Teague, Problems in Modeling the Earth's Trapped Radiation Environment, Air Force Geophysics Laboratory, Hanscom AFB, MA, AFGL-TR-78-0130, 1978.

6. Mullen, E.G., M.S. Gussenhoven, K.A. Lynch and D.H. Brautigam, DMSP Dosimetry Data: A Space Measurement and Mapping of Upset Causing Phenomena, IEEE Transactions on Nuclear Science, to be published December 1987.